

SYNAPTIC MECHANISMS

Functional identification of an outwardly rectifying pH- and anesthetic-sensitive leak K⁺ conductance in hippocampal astrocytes

Kuo-Chang Chu,¹ Cheng-Di Chiu,² Tsan-Ting Hsu,¹ Yu-Ming Hsieh,¹ Yu-Yin Huang³ and Cheng-Chang Lien¹¹Institute of Neuroscience and Brain Research Center, National Yang-Ming University, 155, Section 2, Li-Nong St., Taipei 112, Taiwan²Department of Neurosurgery, Taichung Hospital, 199, Section 1, San Min Rd, Taichung, Taiwan³Department of Anesthesiology, Cheng Hsin General Hospital, 45, Cheng Hsin St., Taipei, Taiwan**Keywords:** glia, hippocampus, potassium channel, TASK channel

Abstract

Astrocytes function as spatial K⁺ buffers by expressing a rich repertoire of K⁺ channels. Earlier studies suggest that acid-sensitive tandem-pore K⁺ channels, mainly TWIK-related acid-sensitive K⁺ (TASK) channels, mediate part of the passive astroglial membrane conductance. Here, using a combination of electrophysiology and pharmacology, we investigated the presence of TASK-like conductance in hippocampal astrocytes of rat brain slices. Extracellular pH shifts to below 7.4 (or above 7.4) induced a prominent inward (or outward) current in astrocytes in the presence of tetrodotoxin, a Na⁺ channel blocker, and 4,4'-diisothiocyanatostilbene-2,2'-disulfonate, a Na⁺ – HCO₃⁻ co-transporter blocker. The pH-sensitive current was insensitive to quinine, a potent blocker of tandem-pore K⁺ channels including TWIK-1 and TREK-1 channels. Voltage-clamp analysis revealed that the pH-sensitive current exhibited weak outward rectification with a reversal potential of –112 mV, close to the Nernst equilibrium potential for K⁺. Furthermore, the current–voltage relationship was well fitted with the Goldman–Hodgkin–Katz current equation for the classical open-rectifier 'leak' K⁺ channel. The pH-sensitive K⁺ current was potentiated by TASK channel modulators such as the volatile anesthetic isoflurane but depressed by the local anesthetic bupivacaine. However, unlike TASK channels, the pH-sensitive current was insensitive to Ba²⁺ and quinine. Thus, the molecular identity of the pH-sensitive leak K⁺ channel is unlikely to be attributable to TASK channels. Taken together, our results suggest a novel yet unknown leak K⁺ channel underlying the pH- and anesthetic-sensitive background conductance in hippocampal astrocytes.

Introduction

Alterations in extracellular pH have important effects on neuronal functions (Balestrino & Somjen, 1988; Deitmer & Rose, 1996; Burdakov *et al.*, 2006; Torborg *et al.*, 2006; Williams *et al.*, 2007). Local and global changes in extracellular pH occur under a variety of physiological and pathological conditions, including synaptic transmission, high-frequency action potential discharge, seizures and ischemic stroke (Siesjö *et al.*, 1985; Chesler & Kaila, 1992; Chesler, 2003). It is therefore crucial for neurons and glia to sense and respond to environmental pH variations under physiological and pathological conditions (Xiong *et al.*, 2004; Gao *et al.*, 2005; Ziemann *et al.*, 2008). Ion channels such as acid-sensing ion channels (ASICs) and tandem of P domains in a weak inwardly rectifying K⁺ (TWIK)-related acid-sensitive K⁺ (TASK) channels, which are rapidly modulated by extracellular protons, are best suited for sensing external pH changes in the central nervous system (CNS; Bayliss

et al., 2003; Wemmie *et al.*, 2006; Duprat *et al.*, 2007; Weng *et al.*, 2010).

ASICs, members of the amiloride-sensitive degenerin/epithelial Na⁺ channel (DEG/ENaC) superfamily, serve as pH sensors in neurons (Waldmann *et al.*, 1997; Baron *et al.*, 2002; Benson *et al.*, 2002). Acid-induced opening of ASICs results in transient inward currents, thereby leading to membrane depolarization. Unlike ASICs, extracellular acidification causes closure of TASK channels, which are pH-sensitive background K⁺ channels belonging to the two-pore-domain K⁺ (K_{2P}; also called KCNK) channel family (Goldstein *et al.*, 2001; Bayliss *et al.*, 2003; Duprat *et al.*, 2007). Consistent with the role of TASK channels in setting resting membrane potential (RMP), extracellular acidification inhibits TASK channels, leading to sustained membrane depolarization and neuronal firing, whereas extracellular alkalization activates TASK channels, resulting in membrane hyperpolarization (Taverna *et al.*, 2005; Torborg *et al.*, 2006).

In the CNS, glial cells greatly outnumber neurons and participate in the regulation of acid–base homeostasis through a variety of exchangers and co-transporters (O'Connor *et al.*, 1994; Deitmer & Rose, 1996; Romero & Boron, 1999; Chesler, 2003). In contrast to our

Correspondence: Dr C-C. Lien, as above.
E-mail: celienc@ym.edu.tw

Received 11 October 2009, revised 9 May 2010, accepted 12 May 2010

knowledge of neuronal pH sensing, specific ion channels involved in detecting extracellular pH variations in astrocytes remain poorly understood. Expression of TASK subunits was strongly detected in astrocytes of several brain regions including the hippocampus (Kindler *et al.*, 2000; Rusznák *et al.*, 2004; Kim *et al.*, 2008). However, the expression of TASK channels in hippocampal astrocytes is controversial because other groups observed that TASK (either TASK-1 or -3) subunits are mainly co-localized with hippocampal neurons (Torborg *et al.*, 2006) and are expressed at a much lower level in astrocytes (Zhou *et al.*, 2009). In agreement with their observations, levels of mRNA expression of these channels in the hippocampal astrocytes *in situ* are unremarkable (Duprat *et al.*, 1997; Talley *et al.*, 2000, 2001; Bayliss *et al.*, 2003).

A major goal of this study is to investigate the functional expression of pH-sensitive leak K^+ channels in hippocampal astrocytes. We demonstrate a TASK-like (modulated by pH and bupivacaine-sensitive) 'leak' K^+ current in hippocampal astrocytes. The current is present after blockade of TWIK-1 and TWIK-related K^+ (TREK)-1 channels, which are believed to be the major background channels in astrocytes (Zhou *et al.*, 2009). Interestingly, unlike TASK channels, the current is insensitive to Ba^{2+} and quinine. Together, these results strongly suggest the presence of other unknown K^+ channels rather than TASK channels underlying the pH- and anesthetic-sensitive leak K^+ conductance in hippocampal astrocytes.

Materials and methods

Preparation of hippocampal slices

Transverse hippocampal slices (200–300 μm thick) were prepared from male Sprague–Dawley rats (postnatal days 22–29) using a vibrating tissue slicer (DSK-1000; Dosaka, Kyoto, Japan) as described previously (Lien *et al.*, 2002; Lien & Jonas, 2003). Animals were killed by rapid decapitation in accordance with national and institutional guidelines (AVMA Guidelines on Euthanasia, June 2007). The experimental design was approved by the Animal Care and Use Committee of National Yang-Ming University. Slices were sectioned in ice-cold artificial cerebrospinal fluid (ACSF) containing (in mM): NaCl, 125; NaHCO_3 , 25; NaH_2PO_4 , 1.25; KCl, 2.5; glucose, 25; CaCl_2 , 2; and MgCl_2 , 1. Following sectioning, slices were incubated in the oxygenated (95% O_2 , 5% CO_2) solution containing (in mM): NaCl, 87; NaHCO_3 , 25; NaH_2PO_4 , 1.25; KCl, 2.5; glucose, 10; sucrose, 75; CaCl_2 , 0.5; and MgCl_2 , 7, with 0.5 μM sulforhodamine 101 (SR101) at 34°C for 25 min. All slices were then transferred to oxygenated solution lacking SR101 at 34°C for 5 min (Kafitz *et al.*, 2008) and finally were stored at room temperature until used. During experiments, slices were placed in a recording chamber and superfused with oxygenated ACSF.

Electrophysiology

Recording electrodes (4–6 $\text{M}\Omega$) were pulled from borosilicate glass (outer diameter 1.5 mm, inner diameter 0.86 mm; Harvard apparatus, Holliston, MA, USA). Experiments were performed under visual control using an Olympus microscope (BX51WI; Tokyo, Japan) equipped with infrared differential interference contrast (IR-DIC) optics (Stuart *et al.*, 1993). Astrocytes with red fluorescence signals in the stratum radiatum of the CA1 area or in the molecular layer of dentate gyrus were selected for recordings. Whole-cell patch recordings were made as described previously (Lien *et al.*, 2002), using an Axopatch 200B amplifier (Molecular Devices, Union City, CA, USA). Pipette capacitance was compensated. The access resistance

($\leq 12 \text{ M}\Omega$) was carefully compensated (correction $\sim 90\%$ with a 35- μs lag). Dual-patch whole-cell recording was used to test the voltage clamp condition (supplementary Fig. S1, A). The left electrode in V-clamp mode was used to deliver the command voltage (V_{cmd} ; supplementary Fig. S1, B) and the right electrode in I-clamp mode was used as a potentiometer to record the actual measured membrane potential (V_{m}) without injecting any current. The V-clamping error, as defined by $(\Delta V_{\text{cmd}} - \Delta V_{\text{m}})/\Delta V_{\text{cmd}}$, was tested by dual-patch recording and was $< 10\%$ ($3.7 \pm 2.1\%$, $n = 7$; supplementary Fig. S1) after the access resistance compensation. Data acquisition (low-pass-filtered at 5 kHz and digitized at 10 kHz) and pulse generation were performed using a Digidata 1440A and pClamp 10.2 software (Molecular Devices). The recording temperature was 21–24°C.

Focal puffs of H^+

Focal puffs of H^+ (duration 5–30 s with 5–10 psi) used to evoke currents in astrocytes (V-clamp potential = -80 mV) were performed with a PicoSpritzer III (Parker Instrumentation, Pine Brook, NJ, USA). Either low/high pH buffers or agonist/antagonist-containing saline was injected via a patch pipette with a wide open tip (2.5–5.0 μm). The PicoSpritzer was triggered by an external TTL pulse generated by Digidata 1440A.

Solutions and drugs

The K^+ -rich internal solution for recording pipettes contained (in mM): Kgluconate, 135; KCl, 20; EGTA, 0.1; MgCl_2 , 2; Na_2ATP , 4; and HEPES, 10; pH was adjusted to 7.3 with KOH. In most experiments (particularly the measurement of I - V relationship), 0.1 mM spermine was added to the internal solution. 2-(*N*-morpholino)ethanesulfonic acid (MES)-buffered saline used for acid pH puff containing (mM): NaCl, 140; KCl, 2.5; CaCl_2 , 2; MgCl_2 , 1; and MES, 10; pH was adjusted to desired pH values with *N*-methyl-D-glucamine (NMDG; Baron *et al.*, 2002; Benson *et al.*, 2002). For alkaline pH puff, MES was replaced with HEPES. For high (or low)- $[\text{Ca}^{2+}]_o$ experiments (Fig. 4A), modified ACSF contained (in mM): NaCl, 125; KCl, 2.5; NaHCO_3 , 25; NaH_2PO_4 , 1.25; CaCl_2 , 2 (or 0.5); MgCl_2 , 1 (or 2.5); and glucose, 25. For low- $[\text{Na}^+]_o$ experiments (Fig. 4B), the ACSF was replaced with a solution containing (in mM): NMDGCl, 120; NaHCO_3 , 25; NaH_2PO_4 , 1.25; KCl, 2.5; CaCl_2 , 2; MgCl_2 , 1; glucose, 25; and sucrose, 15 (pH 7.4). For high- $[\text{K}^+]_o$ experiments (Fig. 4E), modified ACSF contained (in mM): NaCl, 100; KCl, 25; NaHCO_3 , 25; NaH_2PO_4 , 1.25; CaCl_2 , 2; MgCl_2 , 1; and glucose, 25. In all experiments, 0.5 μM tetrodotoxin (TTX; Sigma) and 0.3 mM 4,4'-diisothiocyanatostilbene-2,2'-disulfonate (DIDS) were always added to the bath solution to block voltage-gated Na^+ channels and $\text{Na}^+ - \text{HCO}_3^-$ transporters, respectively. In most experiments, 1 mM kynurenic acid (Sigma or Ascent Scientific, Weston-super-Mare, UK) and 1 μM SR95531 (Tocris Bioscience, Park Ellisville, MO, USA) were included to block AMPA-, NMDA- and GABA_A-receptor-mediated synaptic transmission, respectively. For measuring the reversal potential (E_{rev}), K^+ channel blockers such as tetraethylammonium (TEA; 10 mM) and 4-aminopyrimidine (4-AP; 1 mM) in addition to TTX (0.5 μM), DIDS (0.3 mM), kynurenic acid (1 mM) and SR95531 (1 μM) were added to increase input resistance (R_{in}) of astrocytes, thereby improving the voltage-clamp condition. Amiloride was from Tocris Bioscience, isoflurane was from Alfa Aesar (Ward Hill, MA, USA) and Abbott (Kent, England, UK). All other chemicals were obtained from Sigma, unless specified otherwise.

Live and post hoc identification of astrocyte morphology

SR101-labeled astrocytes in live brain slices were examined either with an epifluorescence microscope (Olympus, BX51WI) or with a two-photon/confocal laser excitation microscope (DM6000 CFS; Leica, Wetzlar, Germany). For examination of gap-junction coupling between astrocytes, a single astrocyte per slice was loaded with biocytin (2 mg/mL) during whole-cell recording. After 30 min recording, slices were fixed overnight with 4% paraformaldehyde in phosphate-buffered saline (PBS; 0.1 M, pH 7.3). Following the PBS wash, slices were incubated with fluorescein isothiocyanate (FITC)-conjugated avidin-D (Invitrogen, Eugene, Oregon, USA) in PBS and 0.3% Triton X-100 overnight at 4°C.

Fluorescence immunohistochemistry

Biocytin-filled cells were subsequently fixed overnight with 4% paraformaldehyde in PBS (0.1 M, pH 7.3). After the PBS wash, slices were incubated in the blocking solution (10% normal goat serum) for 30 min and subsequently with a primary monoclonal antibody against glial fibrillary acidic protein (GFAP; mouse, 1:200; Cell Signaling Technology, Danvers, MA, USA) in PBS containing 5% goat serum and 0.3% triton X-100 for 48 h at 4°C. The secondary antibody (goat antimouse Alexa 488; 1:500, Invitrogen) was applied together with Alexa 594-conjugated streptavidin (1:400; Invitrogen) in PBS and 0.3% triton X-100 overnight at 4°C. After washing, slices were embedded in mounting medium Vectashield® (Vector Laboratories, Burlingame, CA, USA). Labeled cells were examined with a two-photon microscope using a pulsed titanium-sapphire laser (Chameleon-Ultra II tuned to 800 nm; Coherent, Portland, OR, USA) attached to a Leica DM6000 CFS that was equipped with 20×, 0.5 numerical aperture (NA) and 63×, 0.9 NA water-immersion (HCX APO L) objectives. The cell morphology was reconstructed from single section images. The voxel size for 20× and 63× objectives were 0.76 and 0.24 μm, respectively. To show colocalization, digitized images were overlaid using Adobe Photoshop CS3.

Data analysis and statistics

Data analysis was performed with Clampfit 10.2 (Molecular Devices) and GraphPad Prism 5.0 (La Jolla, CA, USA). Traces shown in the figures represent averages of 3–9 sweeps. The concentration–response curve was fitted with the function:

$$f(c) = \frac{E_{\max}}{\left[1 + \left(\frac{EC_{50}}{c}\right)^n\right]} \quad (1)$$

where E_{\max} denotes the maximal effect, c denotes the concentration and EC_{50} represents the half-maximal effective concentration.

The equilibrium potential for K⁺ (E_k) was predicted by the Nernst equation:

$$E_k = \frac{RT}{F} \ln \left(\frac{[K^+]_o}{[K^+]_i} \right) \quad (2)$$

where $[K^+]_o$ and $[K^+]_i$ are outer and inner K⁺ concentrations and F , R and T have the standard thermodynamic meanings (Hille, 2001). The K⁺ current–voltage (I – V) curves were fit with the Goldman–Hodgkin–Katz (GHK) current equation:

$$I = P \frac{EF^2}{RT} \frac{[K^+]_o - [K^+]_i \exp\left(-\frac{EF}{RT}\right)}{1 - \exp\left(-\frac{EF}{RT}\right)} \quad (3)$$

where P is the permeability and E is the voltage. Membrane potential values for measurements of E_{rev} were corrected for the voltage-clamping error (measured by dual-patch recording; see Supplementary Fig. S1) and liquid junction potentials (+13.1 mV in $[K^+]_o = 2.5$ mM ACSF and +10.4 mV in $[K^+]_o = 25$ mM high K⁺ saline); the junction potential difference between the puff solution and external ACSF was negligible and was not taken into account (Taverna *et al.*, 2005).

All values are presented as mean ± SEM. Error bars equal SEM. Statistical significance was tested by the nonparametric paired Wilcoxon signed-rank test at the significance level (P) indicated, using GraphPad Prism 5.0.

Results

Red fluorescent dye SR101 is taken up by a subpopulation of glial cells after a brief exposure in the intact brain or acute brain slices (Nimmerjahn *et al.*, 2004; Kafitz *et al.*, 2008). Here, to reliably identify astrocytes for physiological measurements, we combined whole-cell patch recording with SR101-labeling in acute rat hippocampal slices (Fig. 1A₁ and A₂).

Identification of astrocytes in hippocampal slices

We recorded SR101-labelled cells either in the stratum radiatum of the CA1 region (Fig. 1B₁ and B₂) or in the molecular layer of the dentate gyrus (Fig. 1C) from rats of postnatal days 22–29. The majority (> 92%) of SR101-labelled cells in our recordings exhibited characteristics of electrically ‘passive’ astrocytes. As previously described (Kafitz *et al.*, 2008), they displayed the following features: (i) a very negative RMP (-83.8 ± 0.2 mV, $n = 246$; Fig. 1E); (ii) leaky and passive membrane properties with R_{in} of 4.6 ± 0.1 MΩ ($n = 244$; Fig. 1E); (iii) little active conductance and a lack of action potentials when astrocytes were recorded in the whole-cell voltage (V)-clamp and current (I)-clamp recording configurations, respectively (Fig. 1F); (iv) extensive gap-junction coupling among astrocytes was observed because biocytin loaded into the recorded astrocyte was found to spread to surrounding cells (Fig. 1C). In a subset of experiments, we tested the immunoreactivity of recorded SR101-labelled cells for GFAP, the astrocyte-specific marker. Consistent with previous reports (Nimmerjahn *et al.*, 2004; Kafitz *et al.*, 2008), all SR101-labelled (also stained with biocytin) cells were immunopositive for GFAP (Fig. 1D₁–D₃). Also, the GFAP-positive cells were not immunoreactive for NG2, a specific marker for NG2 cells (supplementary Fig. S2).

Local extracellular pH changes induced inward currents in SR101-positive cells

Previous studies showed that hippocampal neurons sense the environmental pH changes via activation of ASICs or modulation of TASK channels (Baron *et al.*, 2002; Askwith *et al.*, 2004; Weng *et al.*, 2004; Taverna *et al.*, 2005; Torborg *et al.*, 2006). Here, we tested the possible astroglial response to extracellular pH changes by application of a pH 4 solution to single astrocytes under whole-cell V-clamp recordings. Because of extensive astrocyte processes, a space-clamping error of the astrocyte may occur while measuring pH-sensitive

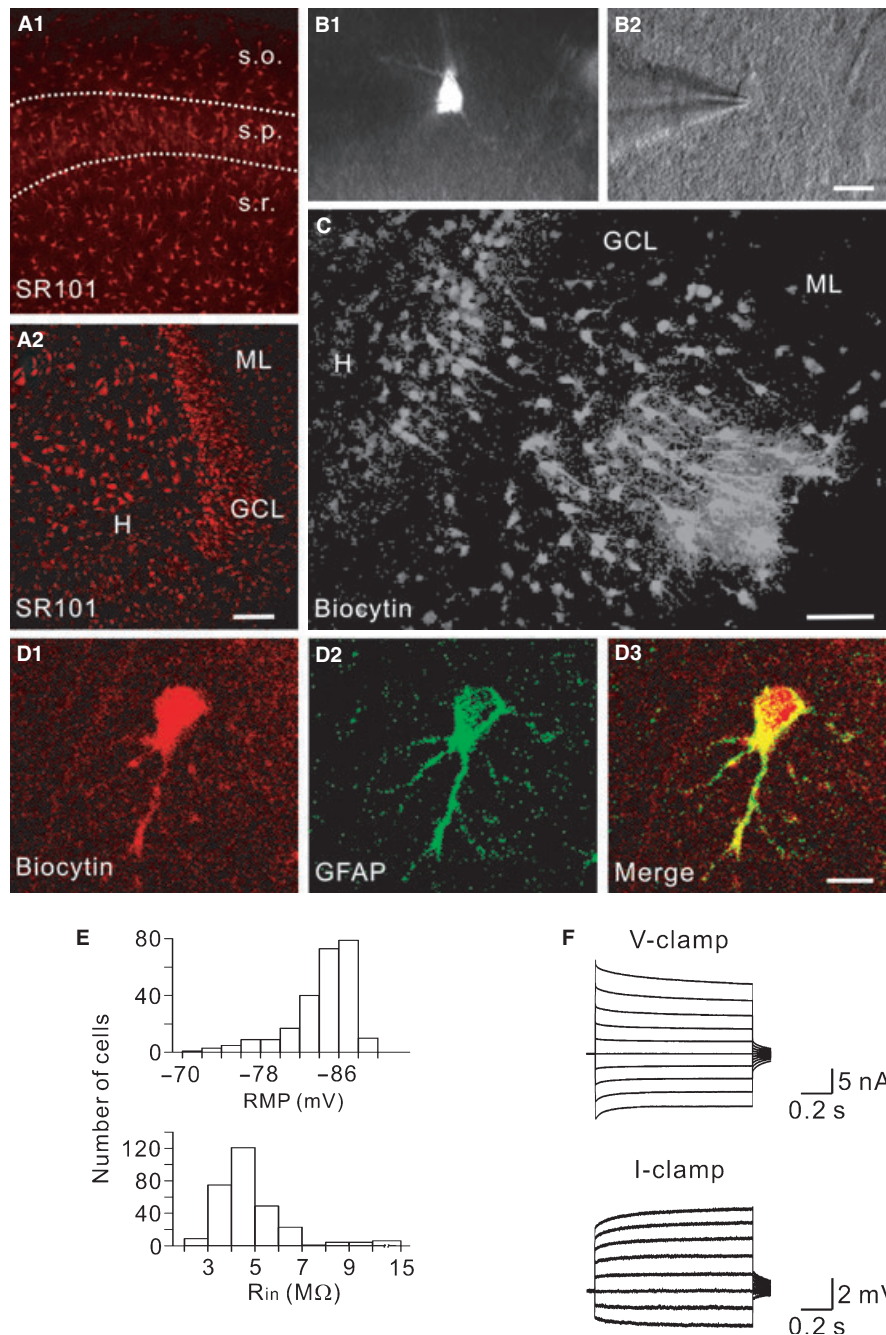


FIG. 1. Identification of astrocytes in the hippocampus. (A) SR101 labeled cells in (A₁) the CA1 region and in (A₂) the dentate gyrus; s.o., stratum oriens; s.p., stratum pyramidale; s.r., stratum radiatum; H, hilus; GCL, granule cell layer; ML, molecular layer. (B) Epifluorescence image of an SR101-labelled cell in the stratum radiatum of the CA1 region (B₁). IR-DIC video image of the same cell with a recording pipette in the whole-cell configuration (B₂). (C) Micrograph showing extensive gap-junction coupling with surrounding astrocytes after filling a single SR101-labelled cell with biocytin and revealed by *post hoc* treatment with FITC-conjugated avidin-D. (D) High-magnification images of (D₁) an Alexa Fluor 594-biocytin stained cell, (D₂) GFAP immunostaining and (D₃) the merged image. (E) Distribution of RMP and R_{in} . (F) Currents activated by 1-s voltage pulses (from -120 mV to -30 mV, 10 mV increments, and holding potential of -80 mV) in the whole-cell voltage (V)-clamp recording (top). Voltage responses to 1-s current pulses (from -800 pA to $+2000$ pA, 400-pA steps, without injecting holding currents) in the whole-cell current (I)-clamp recording (bottom). The same cell as in (B). Scale bars, 250 μ m (A), 10 μ m (B and D), 50 μ m (C).

conductance. To minimize activating extensive pH-sensitive channels at distal processes, we used the focal puff technique to apply a rapid shift in $[H^+]_o$ to the single cell of interest locally. The tip of the puff pipette was placed ~ 15 μ m from the recorded astrocyte (Fig. 2A). A focal puff of pH 4 solution applied to the astrocyte (at V-clamp potential of -80 mV) by a 5-s pulse evoked a prominent sustained inward current (Fig. 2B). The activation and deactivation time

constants of the inward current were 634 ± 48 and 2004 ± 258 ms, respectively ($n = 11$). The effect described here was not mediated by direct activation of mechanosensitive channels because puffs of buffered ACSF (pH 7.4) as a vehicle control did not produced perceived currents (data not shown).

Hippocampal astrocytes exhibit $Na^+ - HCO_3^-$ co-transporters (O'Connor *et al.*, 1994). Focal puffs of low or high pH solutions

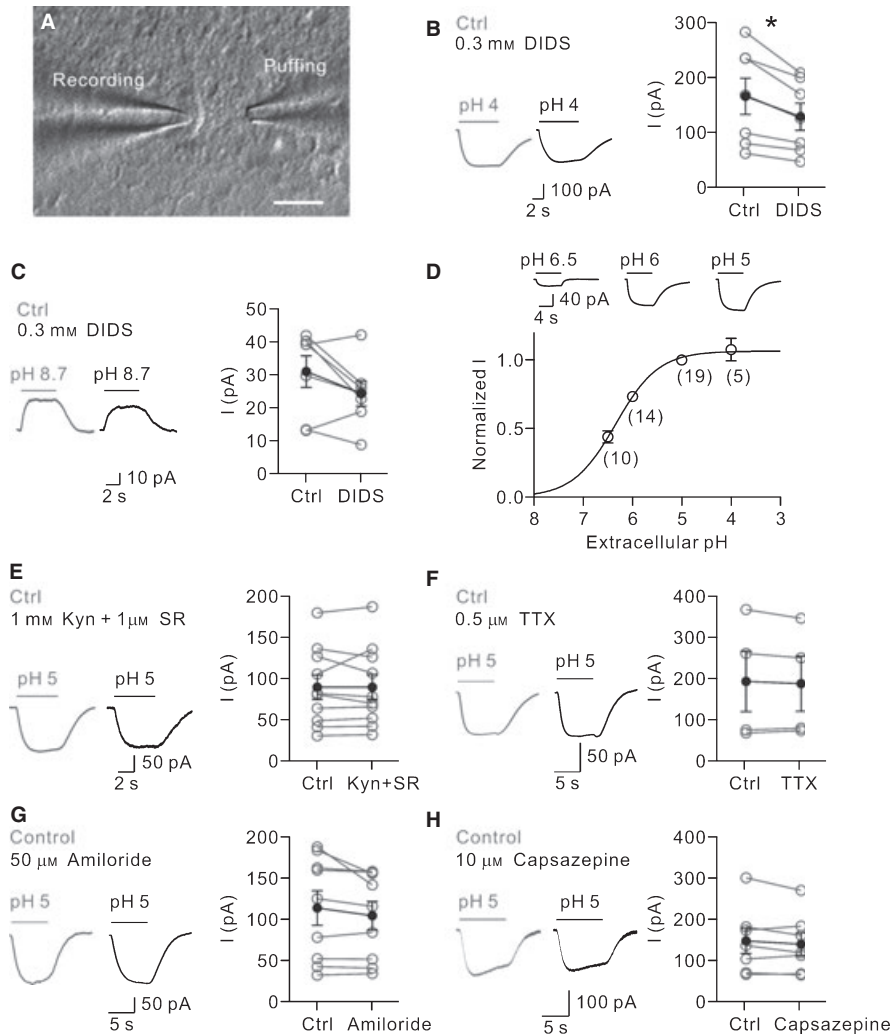


FIG. 2. Focal pH shifts induced sustained currents in astrocytes. (A) IR-DIC image of an astrocyte with a recording pipette and a puffing pipette. (B) Left, focal puffs of pH 4 solution elicited inward currents (V-clamp at -80 mV) in the control (Ctrl) and in the presence of DIDS. Right, summary of the effect of DIDS on the pH 4-evoked currents. $*P < 0.05$. (C) Left, focal puffs of pH 8.7 solution induced outward currents in the Ctrl and in the presence of DIDS. Right, summary of the effect of DIDS on the pH 8.7-evoked currents. (D) Top, inward currents induced by variable pH solutions. Bottom, the dose–response curve showing the pH dependence of evoked currents. Data were fitted with the single Hill equation. The half-maximal effective pH value was 6.3. Numbers of cells are given in parentheses below data points. (E) Left, pH 5-induced currents in the Ctrl and in the presence of kynurenic acid (Kyn) and SR95531 (SR). Right, summary of pH 5-induced currents in the Ctrl and in the presence of TTX. (F) Left, the pH 5-induced current was insensitive to TTX. Right, summary of pH 5-induced currents in the Ctrl and in the presence of amiloride. (G) Left, the pH 5-induced current was insensitive to amiloride. Right, summary of pH 5-induced currents in the Ctrl and in the presence of capsazepine. (H) Left, the pH 5-induced current was insensitive to capsazepine. Right, summary of pH 5-induced currents in the Ctrl and in the presence of capsazepine. Scale bar in A, $10 \mu\text{m}$.

may profoundly perturb extracellular HCO_3^- homeostasis or change intracellular pH values and then cause inward or outward currents in hippocampal astrocytes by activating electrogenic $\text{Na}^+ - \text{HCO}_3^-$ co-transporters. Therefore, we first examined whether these inward currents were generated by electrogenic $\text{Na}^+ - \text{HCO}_3^-$ co-transporters by bath application of 0.3 mM DIDS, which is known to completely block $\text{Na}^+ - \text{HCO}_3^-$ co-transporters (O'Connor *et al.*, 1994). Although bath application of DIDS significantly decreased the inward currents (Fig 2B, left), it revealed that a large fraction ($\sim 79\%$) of currents are DIDS-insensitive ($-166 \pm 33 \text{ pA}$ in the control (Ctrl); $-129 \pm 25 \text{ pA}$ in the presence of DIDS, $n = 7$; $P < 0.05$, Wilcoxon signed-rank test; Fig. 2B, right). In contrast to the effect of pH 4 solution, local puffs of pH 8.7 solution to the astrocyte induced an outward and relatively small current (Fig. 2C, left), which was insensitive to DIDS (Ctrl, $31.0 \pm 4.8 \text{ pA}$; DIDS, $24.3 \pm 3.8 \text{ pA}$, $n = 7$; $P > 0.05$, Wilcoxon signed-rank test; Fig. 2C, right). Because of the substantial contribu-

tion ($\sim 21\%$) of $\text{Na}^+ - \text{HCO}_3^-$ co-transporters in acid-evoked currents, all subsequent experiments were then performed in the presence of 0.3 mM DIDS. Finally, we examined the pH-dependent effect on the magnitude of inward currents by applying different pH solutions to the same astrocytes (Fig. 2D, top traces). The acid-evoked currents were normalized to the current evoked by pH 5 and are shown in Fig. 2D. Data points in Fig. 2D were fitted with Equation (1), yielding a half-maximal effective pH value of 6.3.

Extracellular acidification is known to cause membrane depolarization of either principal neurons or inhibitory interneurons (Taverna *et al.*, 2005; Torborg *et al.*, 2006; Ziemann *et al.*, 2008). To eliminate the influence of network communications, we performed the same experiments in the presence of synaptic blockers and a sodium channel blocker, TTX. The inward currents induced by the focal puffs of H^+ did not differ between the presences of kynurenic acid (Kyn; 1 mM), a broad-spectrum blocker of ionotropic glutamate receptors, and

SR95531 (SR; 1 μM), a selective blocker of γ -aminobutyric acid (GABA) type A (GABA_A) receptors (Ctrl, -90 ± 15 pA; Kyn + SR, -90 ± 15 pA; $n = 10$; $P > 0.05$, Wilcoxon signed-rank test; Fig. 2E). Similar results were also obtained in the presence of 0.5 μM TTX (Ctrl, -193 ± 74 ; TTX, -188 ± 67 pA; $n = 4$; $P > 0.05$, Wilcoxon signed-rank test; Fig. 2F).

One potential mechanism by which H^+ induced an inward current in the glia is through the activation of ASICs. ASICs are expressed in subpopulations of glia (Brockway *et al.*, 2002; Feldman *et al.*, 2008), but it is unknown whether ASICs are expressed in hippocampal astrocytes or are involved in the inward current recorded here. To test the possible involvement of ASICs, we performed the same experiments in the presence of the DEG/ENaC blocker, amiloride. In contrast to the effect of amiloride on ASICs in neurons (Waldmann *et al.*, 1997; see our data in Weng *et al.*, 2010), amiloride (50 μM) failed to inhibit the inward current in astrocytes (Ctrl, -113 ± 21 pA; amiloride, -103 ± 17 pA; $n = 9$; $P > 0.05$, Wilcoxon signed-rank test; Fig. 2G). Furthermore, we tested whether the inward current was mediated by transient receptor potential (TRP) channels as the TRP family subtype TRPV1 is sensitive to extracellular protons (Dhaka *et al.*, 2006). Capsazepine (10 μM), known to block TRPV1 channels, had no effect on the H^+ -induced inward current (Ctrl, -147 ± 31 pA; capsazepine, -139 ± 27 pA; $n = 7$; $P > 0.05$, Wilcoxon signed-rank test; Fig. 2H). Taken together, our results excluded possible involvements of proton-gated cation channels such as ASICs and TRP channels in the acid-induced inward current.

Proton-induced current was insensitive to quinine

A recent report showed that TWIK-1 and TREK-1 channels contribute to astrocyte passive conductance (Zhou *et al.*, 2009). We thus examined the pH-sensitive currents in the presence of quinine, which is known to potently inhibit TWIK-1 and TREK-1 channels. Similar to their report, quinine (200 μM) inhibited astrocytic passive conductance by 31% (Fig. 3A and B). The inhibition is similar to the

blockade of TWIK-1 and TREK-1 currents in astrocytes (Zhou *et al.*, 2009). Furthermore, quinine reversibly inhibited the resting current with a concomitant increase in R_{in} (Fig. 3C). Notably, the inward current induced by the focal puffs of H^+ were not different in the presence of quinine (Ctrl, -279 ± 121 pA; quinine, -190 ± 131 pA; $n = 5$; $P > 0.05$, Wilcoxon signed-rank test; Fig. 3D). Taken together, pH-sensitive currents were unlikely to be mediated by TWIK-1 and TREK-1 channels.

Proton inhibited background K^+ currents

Consistent with the findings that H^+ -gated cation channels (i.e. ASIC and TRPV) are not involved in H^+ -induced inward currents, an increase in $[\text{Ca}^{2+}]_o$ from 0.5 to 2 mM had little effect on H^+ -induced currents (0.5 mM $[\text{Ca}^{2+}]_o$, -111 ± 32 pA; 2 mM $[\text{Ca}^{2+}]_o$, -113 ± 36 pA; $n = 3$; $P > 0.05$, Wilcoxon signed-rank test; Fig. 4A). Furthermore, inward currents were not abolished in low $[\text{Na}^+]_o$ (26 mM) ACSF, in which the majority of Na^+ ions were substituted by NMDG (151 mM $[\text{Na}^+]_o$, -179 ± 6.0 pA; 26 mM $[\text{Na}^+]_o$, -140 ± 19 pA; $n = 3$; $P > 0.05$, Wilcoxon signed-rank test; Fig. 4B). Astrocytes have a large resting conductance and express a rich repertoire of K^+ channels (Butt & Kalsi, 2006). Another possible mechanism underlying the generation of apparent 'inward' currents is through the inhibition of sustained outward background K^+ conductance. To test this hypothesis, we measured the E_{rev} of pH-sensitive current, using a voltage-clamp protocol stepped from -120 to -30 mV. The pH-sensitive component was isolated by subtracting the current evoked in the pH 5 solution from that under the control condition of pH 7.4 (Fig. 4C). To measure the I - V relationship, we selected astrocytes with the access resistance ≤ 12 M Ω for the subsequent analysis. The subtracted current exhibited weakly outward rectification with the E_{rev} close to the equilibrium potential (E_k) for K^+ (measured -112 ± 2 mV, $n = 14$, Fig. 4D inset; calculated E_k , -105 mV). The I - V relationship of the pH-sensitive current was well described by the GHK current equation (open circles, $n = 8$; Fig. 4D),

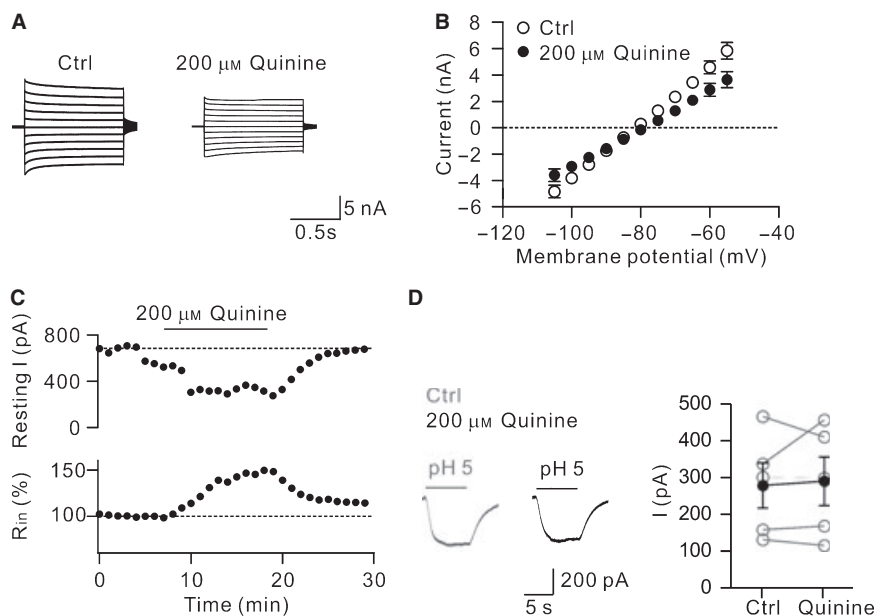


FIG. 3. Proton-induced currents were insensitive to quinine. (A) Representative astrocyte whole-cell passive currents recorded first in the Ctrl and then after addition of 200 μM quinine. Voltage protocol: 1-s voltage pulses (from -105 mV to -55 mV, 5 mV increments, and holding potential of -80 mV). (B) I - V relationship shows that 200 μM quinine inhibited 31% of passive currents. (C) Bath perfusion of 200 μM quinine caused reversible inhibition of the resting current, concomitant with the increase in R_{in} . The dotted lines indicate the mean resting current and normalized mean R_{in} before application of quinine. (D) Left, pH 5-induced currents in the Ctrl and in the presence of quinine. Right, summary of pH 5-induced currents in the Ctrl and in the presence of quinine.

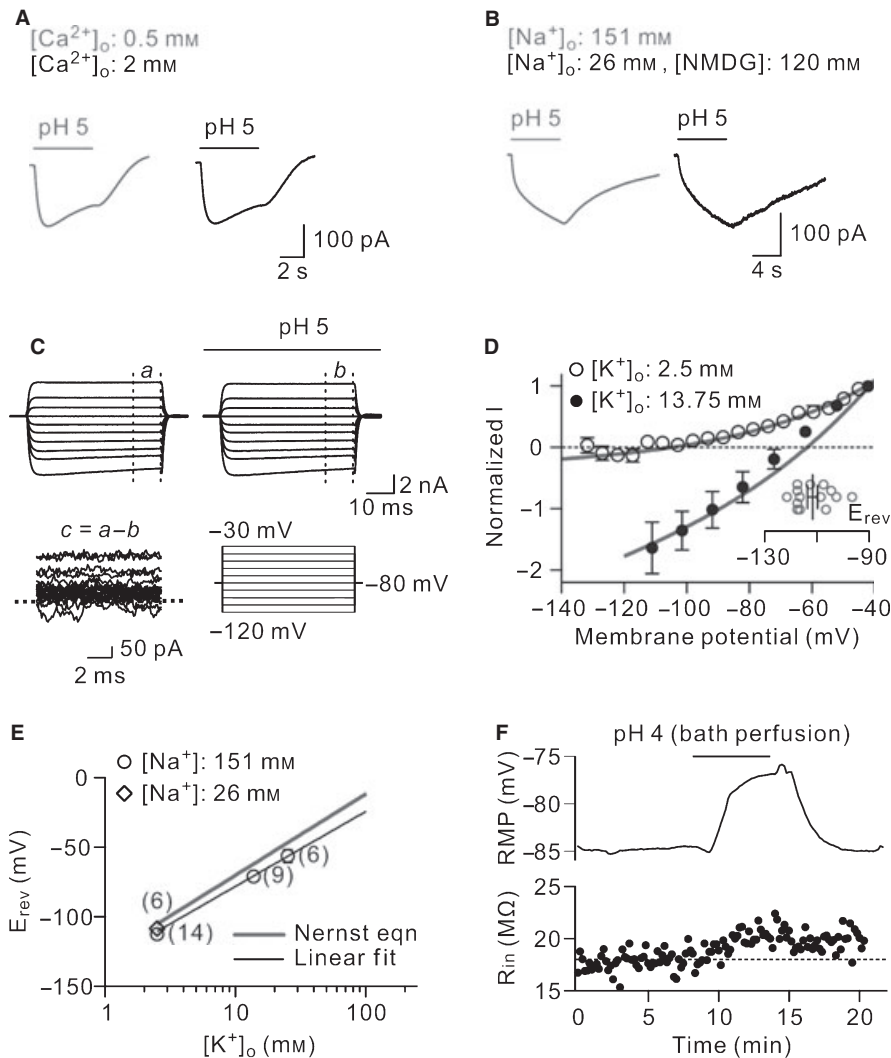


FIG. 4. Proton-induced currents were mediated by inhibition of K⁺ conductance. (A) pH 5-induced inward currents (V-clamp at -80 mV) in (left) low and (right) high $[Ca^{2+}]_o$. (B) pH 5-induced inward currents in $[Na^+]_o = 151$ mM ACSF (left) and NMDG-substituted low Na^+ ACSF (right). (C) Currents evoked by a voltage command protocol (bottom right) stepped from -120 mV to -30 mV with 10-mV increments in the Ctrl (pH 7.4, top left) and during application of H⁺ (pH 5, top right). The vertical dashed lines depict the steady-state currents in the Ctrl (a) and under pH 5 application (b). The currents (c) used for the $I-V$ plot were obtained by digitally subtracting b from a. The horizontal dashed line indicates zero current. (D) $I-V$ relationship of the pH-sensitive current (taken from the average of c) showing weak outward rectification with the E_{rev} at -106 mV (open circles). The dashed line indicates zero current. Inset, the reversal potentials of pH-sensitive currents. Filled circles, the $I-V$ relationship obtained in elevated extracellular $[K^+]_o$. Data were fitted with the GHK current equation. Note the remarkable shift in E_{rev} in elevated $[K^+]_o$. (E) Semilogarithmic plot of the E_{rev} against $[K^+]_o$. The shift in E_{rev} depends on $[K^+]_o$. The continuous lines indicate the calculated E_k predicted by Equation (2) (gray) and the linear fit (black) to the measured E_k . The slope values of the relationship between E_{rev} and $\text{Log}[K^+]_o$ for the calculated and measured E_{rev} are 58.5 and 54.0 mV, respectively. Numbers of cells are given in parentheses next to data points. (F) Bath perfusion with pH 4 solution caused a reversible depolarization of astrocytic RMP, concomitant with an increase in R_{in} in the presence of KA and SR95531. The dotted line indicates the normalized mean R_{in} before acidification.

revealing the lack of intrinsic voltage sensitivity. Moreover, the $I-V$ relationship in elevated $[K^+]_o$ (13.75 mM) was also well fitted by the GHK current equation (filled circles, $n = 9$; Fig. 4D). The ionic selectivity of this current was further tested by raising $[K^+]_o$ to different levels (Fig. 4E). Semilogarithmic plot of the E_{rev} against $[K^+]_o$ showed that the shifts in E_{rev} (circle symbol) under different $[K^+]_o$ were very close to the prediction of the Nernst equation for a K⁺-selective leak current (Fig. 4E). The lines indicate the E_k predicted by the Nernst equation at 22°C (gray) and the linear fit (black) to the measured E_{rev} . The slope values of the relationship between E_{rev} and $\text{Log}[K^+]_o$ for the E_k and E_{rev} are 58.5 mV and 54.0 mV, respectively. Consistently, low $[Na^+]_o$ (substituted by NMDG) experiments ($E_{rev} = -108.2 \pm 2.5$ mV; $n = 6$; diamond symbol) failed to affect E_{rev} . Consistent with the role of leak K⁺ conductance in regulating the RMP, inhibition of pH-sensitive K⁺ channels by bath perfusion of pH

4 solution resulted in slow RMP depolarization ($\Delta RMP = 7.5$ mV; Fig. 4F, top), concomitant with the increase in R_{in} by 2.4 M Ω (Fig. 4F, bottom) in astrocytes. Overall, RMP was increased from -84.3 ± 0.7 to -79.0 ± 0.9 mV ($n = 11$; $P < 0.005$, Wilcoxon signed-rank test), concomitant with the ΔR_{in} by 16% (from 21 ± 2 to 24 ± 2 M Ω ; $n = 12$; $P < 0.005$, Wilcoxon signed-rank test).

TASK channel modulators stimulated pH-sensitive K⁺ channels

The outwardly rectifying pH-sensitive K⁺ channels in astrocytes described above are reminiscent of TASK channels, a subfamily of K_{2P} channels (Duprat *et al.*, 1997, 2007; Goldstein *et al.*, 2001). A prominent feature of TASK channels is the dichotomous pH effect on the TASK channel conductance (Taverna *et al.*, 2005; Torborg *et al.*, 2006). In the same cell, we showed that pH 4 and pH 8.7

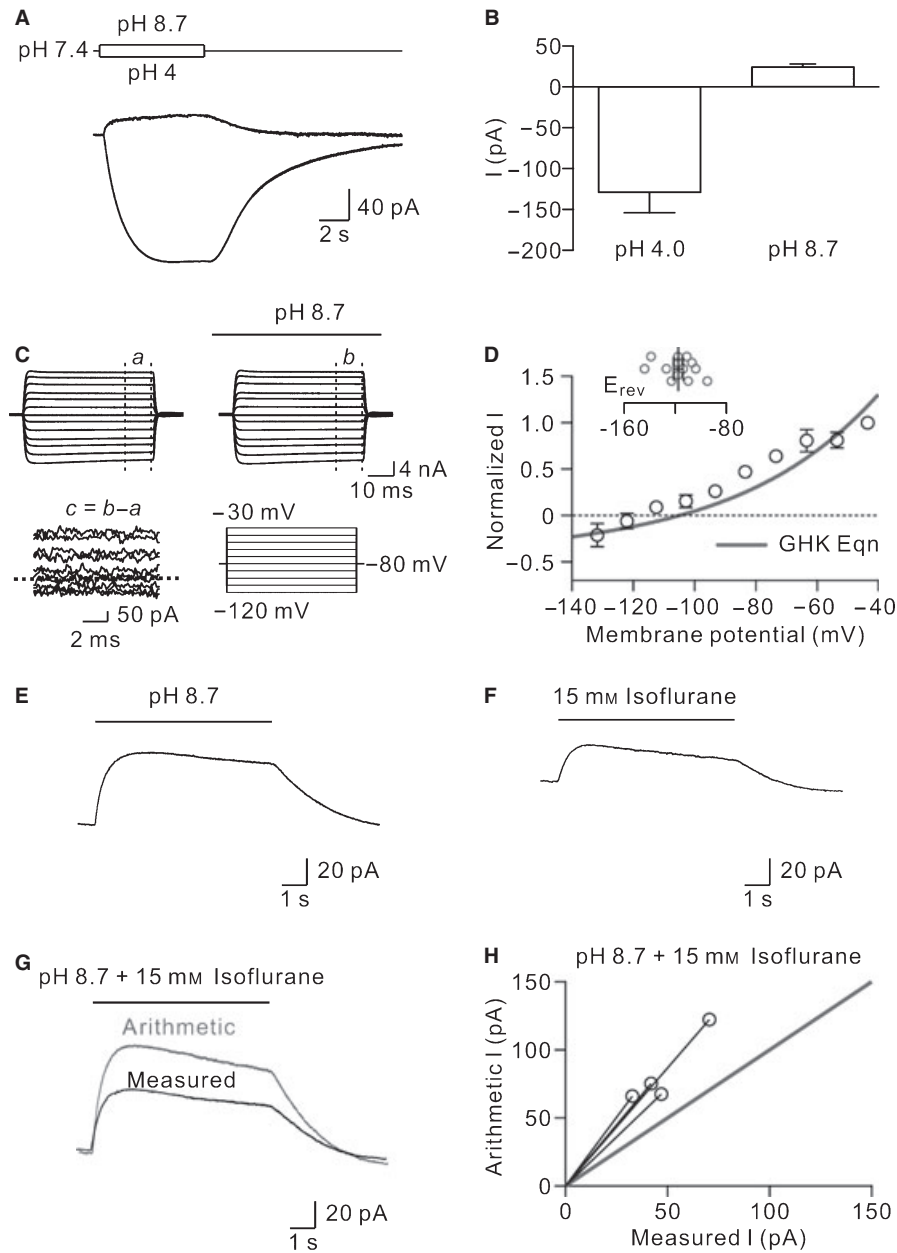


FIG. 5. H^+ -inhibited leak K^+ channel was stimulated by alkaline pH and isoflurane. (A) In the same astrocyte (V-clamp at -80 mV), pH 8.7 induced an outward current whereas pH 4 induced a large inward current. Pulse protocol is shown above the traces. (B) Summary of the mean current evoked by pH 4 and pH 8.7. (C) Currents evoked by a voltage command protocol (bottom right, the same as in Fig. 4C) in the Ctrl (pH 7.4, top left) and during alkalization (pH 8.7, top right). The vertical dashed lines depict the steady-state currents in the Ctrl (*a*) and under pH 8.7 application (*b*), respectively. The current (*c*) was obtained by digitally subtracting *a* from *b*. (D) I - V relationship of the pH 8.7-activated current (*c*) obtained by digital subtraction showing a weak outward rectification with a reversal potential at -105 mV. Fitted line from the GHK current equation is shown superimposed. Inset, the reversal potentials of alkaline-sensitive currents. All recordings were obtained under the same experimental conditions as in Fig. 4D. (E) pH 8.7 induced a prominent outward current. (F) Similar to alkaline pH, isoflurane induced an outward current. (G) Co-application of pH 8.7 and isoflurane induced an outward current far smaller than the arithmetic sum of currents shown in E and F. Traces in E-G are from the same cell. (H) Arithmetic currents calculated by summation of alkaline pH- and isoflurane-induced currents plotted against currents induced by co-application of alkaline and isoflurane. All data points connected to the are above the identity line, indicating a large degree of occlusion between alkaline pH and isoflurane.

evoked sustained currents with opposite polarities (Fig. 5A). Overall, the currents evoked by pH 4 and pH 8.7 were -129.1 ± 24.8 pA and $+24.3 \pm 3.8$, respectively ($n = 7$; Fig. 5B). We therefore examined whether alkaline-evoked outward currents share functional similarities with acid-evoked K^+ currents by measuring the I - V relationship using voltage commands stepping from -120 mV to -30 mV. To obtain the alkaline-activated current, we subtracted the control (pH 7.4) current from the current in the basic (pH 8.7) solution (Fig. 5C). As shown in Fig. 5D, the I - V relationship of the alkaline-sensitive current was

moderately described by the GHK current equation with the E_{rev} (-118 ± 4 mV; $n = 13$; Fig. 5D, inset) close to the calculated E_K . Similar to the alkaline effect (Fig. 5E), focal application of the volatile anesthetic isoflurane (15 mM) also produced a prominent outward current (26.5 ± 7.3 pA; $n = 4$; Fig. 5F). The effect of isoflurane was largely occluded by pH 8.7, because the current evoked by co-application of pH 8.7 and 15 mM isoflurane was markedly smaller than the arithmetic sum of individual effects (measured, 70.6 pA; arithmetic sum, 122.5 pA; Fig. 5G). Figure 5H plots the arithmetic

current calculated by summation of the H⁺-induced current and the isoflurane-induced current against the measured current induced by co-application. All data points connected to the origin are above the identity line. Overall, the measured current of 48.1 ± 8.1 pA ($n = 4$) was significantly smaller than the arithmetic sum current of 82.9 ± 13.3 pA ($n = 4$, $P < 0.05$; Wilcoxon signed-rank test).

Effects of TASK channel blockers

Barium (Ba²⁺) and the local anesthetic bupivacaine are known to block TASK channels (Goldstein *et al.*, 2001; Bayliss *et al.*, 2003; Taverna *et al.*, 2005; Torborg *et al.*, 2006; Duprat *et al.*, 2007). To further highlight the molecular identity of the pH-sensitive K⁺ channel, we tested the inhibitory effects of Ba²⁺ and bupivacaine. Similar to the H⁺-mediated effect (-114 pA by pH 4; Fig. 6A), 1 mM Ba²⁺ inhibited the resting current by -114 pA (Fig. 6B). Co-application of pH 4 solution and Ba²⁺ at a concentration of 1 mM inhibited the resting current by -246 pA (Fig. 6C), similar to the arithmetic sum of the individual effect ('arithmetic' -229 pA). Under this high concentration of Ba²⁺, pH 4 still had an additive effect, indicating that the acid-sensitive current was insensitive to Ba²⁺. Overall, application of pH 4 solution and 1 mM Ba²⁺ inhibited the resting currents by -155 ± 17 pA and -233 ± 28 pA ($n = 9$), respectively, and the summary plot (Fig. 6D) showed the arithmetic current calculated by summation of the H⁺-induced current and the Ba²⁺-induced current against the measured current induced by co-application of the two. The measured current of 391.3 ± 43.9 pA was not significantly different from the arithmetic current of 387.9 ± 40.5 pA ($n = 9$, $P > 0.05$; Wilcoxon signed-rank test). Because 1 mM Ba²⁺ is known to block TASK and inwardly rectifying K⁺ (K_{ir}) channels, a more stringent test to examine the Ba²⁺ sensitivity is to evoke the pH-sensitive current in the presence of bath-applied 1 mM Ba²⁺, TTX (0.5 μ M), DIDS (0.3 mM) and a gap junction blocker, carbenoxolone disodium (Cbx; 100 μ M). Under this condition, focal pH 5 puffs still evoked similar inward currents (Fig. 6E).

Like Ba²⁺, bupivacaine (0.5 mM) alone strongly inhibited resting currents (51 pA; Fig. 6G). However, co-application of bupivacaine and H⁺ evoked a measured inward current of 66.4 pA, significantly less than the arithmetic sum of (171 pA) of the individual effects (Fig. 6H). Figure 6I plots the arithmetic current obtained by summation of the H⁺-induced current and the bupivacaine-induced current against the measured current induced by co-application of H⁺ and bupivacaine. All data points connected to the origin are above the identity line (measured current 143.6 ± 16.0 pA, arithmetic current 218.0 ± 25.2 pA; $n = 14$, $P < 0.05$; Wilcoxon signed-rank test). These results show a large degree of occlusion between the effects of low pH and bupivacaine.

Discussion

TASK-like K⁺ conductance in astrocytes

The pH-sensitive leak (or background) current recorded from the SR101-labelled astrocytes in the stratum radiatum of the CA1 region and in the molecular layer of the dentate gyrus is characterized by the following properties: (i) The current exhibits weak outward rectification with an E_{rev} of -112 ± 2 mV ($n = 14$), close to the equilibrium potential for K⁺; (ii) its I - V relationship fits well with the GHK current equation for a K⁺-selective leak channel; (iii) the current is inhibited by extracellular acidification but is stimulated by extracellular alkalization; (iv) the current is stimulated by isoflurane but inhibited by bupivacaine. Taken together, the biophysical and pharmacological

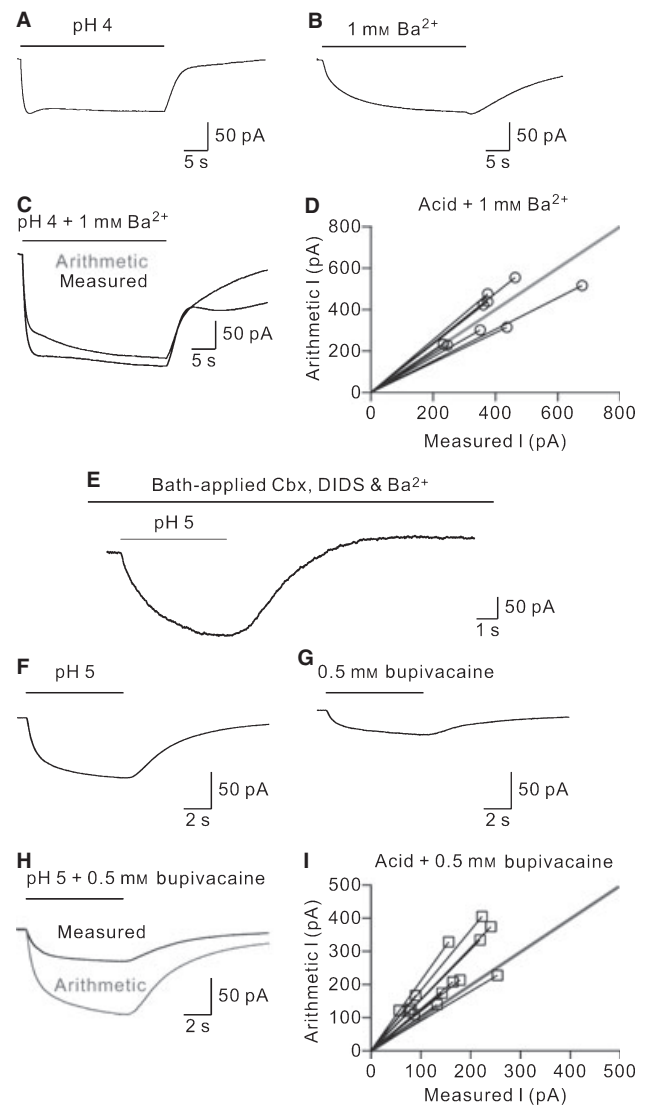


FIG. 6. H⁺-inhibited K⁺ conductance was sensitive to bupivacaine but not Ba²⁺. (A) pH 4-induced inward current in an astrocyte (V-clamp at -80 mV). (B) 1 mM Ba²⁺-induced inward current from the same cell. (C) Co-application of pH 4 and Ba²⁺ induced an inward current ('measured') similar to the arithmetic summation ('arithmetic') of H⁺-induced current and Ba²⁺-induced current. (D) Expected currents calculated by summation of H⁺-induced current and Ba²⁺-induced current, versus measured currents induced by co-application of H⁺ and Ba²⁺. All data points connected to the axis origin are close to the identity line, indicating a lack of occlusion effect between pH 4 and 1 mM Ba²⁺. (E) A focal puff of pH 5 solution elicited an inward current in the presence of bath-applied Ba²⁺ (1 mM), DIDS (0.3 mM) and Cbx (100 μ M). Cbx was used to improve the voltage clamp. (F) pH 5-induced inward current. (G) 0.5 mM bupivacaine-induced inward current. (H) Current from co-application of pH 5 and bupivacaine ('measured') was significantly smaller than the arithmetic sum of pH 5-induced current and bupivacaine-induced current. (I) Arithmetic currents calculated by summation of H⁺-induced current and bupivacaine-induced current, plotted against measured currents induced by co-application of H⁺ and bupivacaine. All data points connected to the origin are above the identity line, indicating marked occlusion of the effects.

properties of the pH-sensitive current described here are reminiscent of those mediated by recombinant TASK channels expressed in heterologous systems (Patel *et al.*, 1999) and many native TASK channels (Buckler *et al.*, 2000; Sirois *et al.*, 2000; Kang *et al.*, 2004; Taverna *et al.*, 2005; Torborg *et al.*, 2006).

Are TASK channels truly the molecular basis underlying pH-sensitive leak K⁺ currents here? Two lines of evidence in the

present study do not support this view. First, the pH-sensitive current is readily evoked in the presence of 1 mM Ba²⁺, a high concentration known to block TASK and K_{ir} channels (Seifert *et al.*, 2009), indicating the presence of other pH-sensitive leak channels which show insensitivity to Ba²⁺ (Fig. 6D and E). Second, the half-maximal pH value (6.3) is lower than that reported for rTASK-1 (~7.4; Talley *et al.*, 2000) and rTASK-3 (~6.7; Kim *et al.*, 2000). As K_{2P} channels are a relatively new K⁺ channel family with potentially more isoforms to be uncovered, specific K_{2P} channel blockers are needed to establish a precise relationship between passive conductance of astrocytes and specific K_{2P} isoforms in the future.

Comparison to previous work

A recent study showed that TWIK-1 and TREK-1 channels are the major components of the K⁺ channels long thought to underlie the passive conductance of hippocampal astrocytes (Zhou *et al.*, 2009). Obviously, the pH-sensitive open-rectifier K⁺ channel identified in the present study is distinct from them because quinine (200 μM), which potently inhibits TWIK-1 and TREK-1 channels, has no effect on the pH-induced current (Fig. 3D). It remains puzzling why pH- or bupivacaine-sensitive weakly outward rectifying K⁺ currents in hippocampal astrocytes have not been previously reported (Seifert *et al.*, 2009; Zhou *et al.*, 2009). Methodological differences might be one of the reasons. First, perfusion of low-pH bath solutions in the previous work extensively activated all pH-sensitive K⁺ channels in the recorded astrocytes. The linear *I-V* relationship of pH-sensitive K⁺ currents reflects a combination of currents resulting from the superposition of several pH-sensitive components, including TWIK-1, TREK-1 and other K_{2P} channels. Second, the conductance changes at astrocyte processes are not voltage-clamped, rendering the precise measurement of the somatically recorded current amplitudes and kinetics impossible. Third, a substantial contribution (21%) of Na⁺ – HCO₃⁻ co-transporters may confound the measurement of pH-sensitive K⁺ currents. Finally, a proper compensation of access resistance compensation is critical for biophysical analysis of current behavior in astrocytes.

Although changing bath pH is thought to be more reflective of global pH changes associated with pathological conditions such as ischemia, local changes in pH in the present study may be more like the local reductions in pH during synaptic transmission and high-frequency action potential discharge (Chesler & Kaila, 1992). Most importantly, puff application avoids the space-clamp error while measuring the biophysical properties of membrane channels.

Functional implication

Astrocytes are implicated in many neurological disorders (Seifert *et al.*, 2006; Ding *et al.*, 2007; Rossi *et al.*, 2007). Seizures and ischemic stroke can reduce brain pH from 7.35 to ~ 6.7 (Rossi *et al.*, 2007; Ziemann *et al.*, 2008). Therefore, the half-maximal effective pH value (6.3) of astroglial pH-sensitive K⁺ channels in this study would be pathologically relevant. Because of the lack of ASICs in astrocytes, the role of pH-sensitive K⁺ channels in astrocytes during extracellular acidification seems to be particularly important. During brain ischemia, extracellular acidosis and hypoxia can lead to down-regulation of pH-sensitive K⁺ channels in the astrocytes of the ischemic region. Consequently, the membrane potential gradient in the astroglial syncytium is disrupted, leading to dysfunction of homeostatic regulation of [K⁺]_o in the brain (Butt & Kalsi, 2006; Seifert *et al.*, 2006; Rossi *et al.*, 2007). On the other hand, astrocyte membrane

depolarization induced by elevated [K⁺]_o and protons favors astroglial uptake of Na⁺ and HCO₃⁻ through Na⁺ – HCO₃⁻ co-transporters. The resulting increase in intracellular osmolarity drives water into astroglia through aquaporin-4 channels. The inappropriate redistribution of water and ions results in tissue edema and subsequent brain damage. Thus, potentiation of pH-sensitive K⁺ conductance by volatile anesthetics may attenuate [K⁺]_o elevation and tissue edema. Intriguingly, volatile anesthetics and polyunsaturated fatty acids that have been shown to prevent neuronal death in animal models of ischemia may exert their action by modulating leakage K⁺ channels (Lauritzen *et al.*, 2000). Future work on the definitive identification of the molecular nature of pH-sensitive K⁺ channels and how significantly the activity of them contributes to the overall astrocyte passive conductance are needed. Also, the development of selective blockers is necessary and may be potentially useful for preventing brain edema and ischemic brain damage (Bayliss & Barrett, 2008).

Supporting Information

Additional supporting information may be found in the online version of this article:

Data S1. Materials and methods. Functional identification of an outwardly rectifying pH- and anesthetic-sensitive leak K⁺ conductance in hippocampal astrocytes.

Fig. S1. Estimation of voltage-clamping errors in astrocytes.

Fig. S2. No co-localization of GFAP and NG-2 immunoreactivities.

Please note: As a service to our authors and readers, this journal provides supporting information supplied by the authors. Such materials are peer-reviewed and may be re-organized for online delivery, but are not copy-edited or typeset by Wiley-Blackwell. Technical support issues arising from supporting information (other than missing files) should be addressed to the authors.

Acknowledgements

We thank C. Chen and Drs M.-M. Poo and C. Hung for critically reading the manuscript and Drs U. Kraushaar and M. Martina for their comments on the experiments. This work was supported by the Ministry of Education, Taiwan (Aim for The Top University Plan), National Health Research Institutes (Grants NHRI-EX97-9720NC), Taiwan National Science Council (Grant 96-2320-B-010-010-MY2), Yen Tjing Ling Medical Foundation (CI-96-4) and VGHUST Joint Research Program, Tsou's Foundation Grant VGHUST97-P6-29.

Abbreviations

4-AP, 4-aminopyridine; AMPA, α-amino-3-hydroxy-5-methyl-4-isoxazole-propionic acid; ASIC, acid-sensing ion channel; Cbx, carbenoxolone disodium; CNS, central nervous system; Ctrl, control; DEG/ENaC, degenerin/epithelial Na⁺ channel; DIDS, 4,4'-diisothiocyanatostilbene-2,2'-disulfonate; FITC, fluorescein isothiocyanate; GABA, γ-aminobutyric acid; GFAP, glial fibrillary acidic protein; GHK, Goldman-Hodgkin-Katz; IR-DIC, infrared differential interference contrast; K_{2P}, two-pore-domain K⁺; K_{ir}, inwardly rectifying K⁺; MES, 2-(*N*-morpholino)ethanesulfonic acid; NMDA, *N*-methyl-D-aspartate; NMDG, *N*-methyl-D-glucamine; PBS, phosphate-buffered saline; R_{in}, input resistance; RMP, resting membrane potential; SR101, sulforhodamine 101; TASK, TWIK-related acid-sensitive K⁺; TEA, tetraethylammonium; TREK, TWIK-related K⁺; TRP, transient receptor potential¹ TTX, tetrodotoxin; TWIK, tandem of P domains in a weak inwardly rectifying K⁺.

References

- Askwith, C.C., Wemmie, J.A., Price, M.P., Rokhlina, T. & Welsh, M.J. (2004) Acid-sensing ion channel 2 (ASIC2) modulates ASIC1 H⁺-activated currents in hippocampal neurons. *J. Biol. Chem.*, **279**, 18296–18305.

- Balestrino, M. & Somjen, G.G. (1988) Concentration of carbon dioxide, interstitial pH and synaptic transmission in hippocampal formation of the rat. *J. Physiol.*, **396**, 247–266.
- Baron, A., Waldmann, R. & Lazdunski, M. (2002) ASIC-like, proton-activated currents in rat hippocampal neurons. *J. Physiol.*, **539**, 485–494.
- Bayliss, D.A. & Barrett, P.Q. (2008) Emerging roles for two-pore-domain potassium channels and their potential therapeutic impact. *Trends Pharmacol. Sci.*, **29**, 566–575.
- Bayliss, D.A., Sirois, J.E. & Talley, E.M. (2003) The TASK family: two-pore domain background K⁺ channels. *Mol. Interv.*, **3**, 205–219.
- Benson, C.J., Xie, J., Wemmie, J.A., Price, M.P., Henss, J.M., Welsh, M.J. & Snyder, P.M. (2002) Heteromultimers of DEG/ENaC subunits form H⁺-gated channels in mouse sensory neurons. *Proc. Natl Acad. Sci. USA*, **99**, 2338–2343.
- Brockway, L.M., Zhou, Z.H., Bubien, J.K., Jovov, B., Benos, D.J. & Keyser, K.T. (2002) Rabbit retinal neurons and glia express a variety of ENaC/DEG subunits. *Am. J. Physiol. Cell Physiol.*, **283**, C126–C134.
- Buckler, K.J., Williams, B.A. & Honore, E. (2000) An oxygen-, acid- and anaesthetic-sensitive TASK-like background potassium channel in rat arterial chemoreceptor cells. *J. Physiol.*, **525**, 135–142.
- Burdakov, D., Jensen, L.T., Alexopoulos, H., Williams, R.H., Fearon, I.M., O'Kelly, I., Gerasimenko, O., Fugger, L. & Verkhratsky, A. (2006) Tandem-pore K⁺ channels mediate inhibition of orexin neurons by glucose. *Neuron*, **50**, 711–722.
- Butt, A.M. & Kalsi, A. (2006) Inwardly rectifying potassium channels (Kir) in central nervous system glia: a special role for Kir4.1 in glial functions. *J. Cell Mol. Med.*, **10**, 33–44.
- Chesler, M. (2003) Regulation and modulation of pH in the brain. *Physiol. Rev.*, **83**, 1183–1221.
- Chesler, M. & Kaila, K. (1992) Modulation of pH by neuronal activity. *Trends Neurosci.*, **15**, 396–402.
- Deitmer, J.W. & Rose, C.R. (1996) pH regulation and proton signalling by glial cells. *Prog. Neurobiol.*, **48**, 73–103.
- Dhaka, A., Viswanath, V. & Patapoutian, A. (2006) TRP ion channels and temperature sensation. *Annu. Rev. Neurosci.*, **29**, 135–161.
- Ding, S., Fellin, T., Zhu, Y., Lee, S.Y., Auberson, Y.P., Meaney, D.F., Coulter, D.A., Carmignoto, G. & Haydon, P.G. (2007) Enhanced astrocytic Ca²⁺ signals contribute to neuronal excitotoxicity after status epilepticus. *J. Neurosci.*, **27**, 10674–10684.
- Duprat, F., Lesage, F., Fink, M., Reyes, R., Heurteaux, C. & Lazdunski, M. (1997) TASK, a human background K⁺ channel to sense external pH variations near physiological pH. *EMBO J.*, **16**, 5464–5471.
- Duprat, F., Lauritzen, I., Patel, A. & Honoré, E. (2007) The TASK background K₂P channels: chemo- and nutrient sensors. *Trends Neurosci.*, **30**, 573–580.
- Feldman, D.H., Horiuchi, M., Keachie, K., Mccauley, E., Bannerman, P., Itoh, A., Itoh, T. & Pleasure, D. (2008) Characterization of acid-sensing ion channel expression in oligodendrocyte-lineage cells. *Glia*, **56**, 1238–1249.
- Gao, J., Duan, B., Wang, D.G., Deng, X.H., Zhang, G.Y., Xu, L. & Xu, T.L. (2005) Coupling between NMDA receptor and acid-sensing ion channel contributes to ischemic neuronal death. *Neuron*, **48**, 635–646.
- Goldstein, S.A., Bockenbauer, D., O'Kelly, I. & Zilberberg, N. (2001) Potassium leak channels and the KCNK family of two-P-domain subunits. *Nat. Rev. Neurosci.*, **2**, 175–184.
- Hille, B. (2001) *Ion channels of excitable membranes*. Sinauer, Sunderland, MA.
- Kafitz, K.W., Meier, S.D., Stephan, J. & Rose, C.R. (2008) Developmental profile and properties of sulforhodamine 101-labeled glial cells in acute brain slices of rat hippocampus. *J. Neurosci. Methods*, **169**, 84–92.
- Kang, D., Han, J., Talley, E.M., Bayliss, D.A. & Kim, D. (2004) Functional expression of TASK-1/TASK-3 heteromers in cerebellar granule cells. *J. Physiol.*, **554**, 64–77.
- Kim, Y., Bang, H. & Kim, D. (2000) TASK-3, a new member of the tandem pore K⁺ channel family. *J. Biol. Chem.*, **275**, 9340–9347.
- Kim, J.E., Kwak, S.E., Choi, S.Y. & Kang, T.C. (2008) Region-specific alterations in astroglial TWIK-related acid-sensitive K⁺-1 channel immunoreactivity in the rat hippocampal complex following pilocarpine-induced status epilepticus. *J. Comp. Neurol.*, **510**, 463–474.
- Kindler, C.H., Pietruck, C., Yost, C.S., Sampson, E.R. & Gray, A.T. (2000) Localization of the tandem pore domain K⁺ channel TASK-1 in the rat central nervous system. *Brain Res. Mol. Brain Res.*, **80**, 99–108.
- Lauritzen, I., Blondeau, N., Heurteaux, C., Widmann, C., Romey, G. & Lazdunski, M. (2000) Polyunsaturated fatty acids are potent neuroprotectors. *EMBO J.*, **19**, 1784–1793.
- Lien, C.C. & Jonas, P. (2003) Kv3 potassium conductance is necessary and kinetically optimized for high-frequency action potential generation in hippocampal interneurons. *J. Neurosci.*, **23**, 2058–2068.
- Lien, C.C., Martina, M., Schultz, J.H., Ehmke, H. & Jonas, P. (2002) Gating, modulation and subunit composition of voltage-gated K⁺ channels in dendritic inhibitory interneurons of rat hippocampus. *J. Physiol.*, **538**, 405–419.
- Nimmerjahn, A., Kirchhoff, F., Kerr, J.N. & Helmchen, F. (2004) Sulforhodamine 101 as a specific marker of astroglia in the neocortex *in vivo*. *Nat. Methods*, **1**, 31–37.
- O'Connor, E.R., Sontheimer, H. & Ransom, B.R. (1994) Rat hippocampal astrocytes exhibit electrogenic sodium-bicarbonate co-transport. *J. Neurophysiol.*, **72**, 2580–2589.
- Patel, A.J., Honoré, E., Lesage, F., Fink, M., Romey, G. & Lazdunski, M. (1999) Inhalational anesthetics activate two-pore-domain background K⁺ channels. *Nat. Neurosci.*, **2**, 422–426.
- Romero, M.F. & Boron, W.F. (1999) Electrogenic Na⁺/HCO₃⁻ cotransporters: cloning and physiology. *Annu. Rev. Physiol.*, **61**, 699–723.
- Rossi, D.J., Brady, J.D. & Mohr, C. (2007) Astrocyte metabolism and signaling during brain ischemia. *Nat. Neurosci.*, **10**, 1377–1386.
- Rusznák, Z., Pocsai, K., Kovács, I., Pór, A., Pál, B., Bíró, T. & Szűcs, G. (2004) Differential distribution of TASK-1, TASK-2 and TASK-3 immunoreactivities in the rat and human cerebellum. *Cell. Mol. Life Sci.*, **61**, 1532–1542.
- Seifert, G., Schilling, K. & Steinhäuser, C. (2006) Astrocyte dysfunction in neurological disorders: a molecular perspective. *Nat. Rev. Neurosci.*, **7**, 194–206.
- Seifert, G., Hüttmann, K., Binder, D.K., Hartmann, C., Wyczyński, A., Neusch, C. & Steinhäuser, C. (2009) Analysis of astroglial K⁺ channel expression in the developing hippocampus reveals a predominant role of the Kir4.1 subunit. *J. Neurosci.*, **29**, 7474–7488.
- Siesjö, B.K., von Hanwehr, R., Nergelius, G., Nevander, G. & Ingvar, M. (1985) Extra- and intracellular pH in the brain during seizures and in the recovery period following the arrest of seizure activity. *J. Cereb. Blood Flow Metab.*, **5**, 47–57.
- Sirois, J.E., Lei, Q., Talley, E.M., Lynch, C. III & Bayliss, D.A. (2000) The TASK-1 two-pore domain K⁺ channel is a molecular substrate for neuronal effects of inhalation anesthetics. *J. Neurosci.*, **20**, 6347–6354.
- Stuart, G.J., Dodt, H.U. & Sakmann, B. (1993) Patch-clamp recordings from the soma and dendrites of neurons in brain slices using infrared video microscopy. *Pflügers Arch.*, **423**, 511–518.
- Talley, E.M., Lei, Q., Sirois, J.E. & Bayliss, D.A. (2000) TASK-1, a two-pore domain K⁺ channel, is modulated by multiple neurotransmitters in motoneurons. *Neuron*, **25**, 399–410.
- Talley, E.M., Solórzano, G., Lei, Q., Kim, D. & Bayliss, D.A. (2001) CNS distribution of members of the two-pore-domain (KCNK) potassium channel family. *J. Neurosci.*, **21**, 7491–7505.
- Taverna, S., Tkatch, T., Metz, A.E. & Martina, M. (2005) Differential expression of TASK channels between horizontal interneurons and pyramidal cells of rat hippocampus. *J. Neurosci.*, **25**, 9162–9170.
- Torborg, C.L., Berg, A.P., Jeffries, B.W., Bayliss, D.A. & McBain, C.J. (2006) TASK-like conductances are present within hippocampal CA1 stratum oriens interneuron subpopulations. *J. Neurosci.*, **26**, 7362–7367.
- Waldmann, R., Champigny, G., Bassilana, F., Heurteaux, C. & Lazdunski, M. (1997) A proton-gated cation channel involved in acid-sensing. *Nature*, **386**, 173–177.
- Wemmie, J.A., Price, M.P. & Welsh, M.J. (2006) Acid-sensing ion channels: advances, questions and therapeutic opportunities. *Trends Neurosci.*, **29**, 578–586.
- Weng, X.C., Zheng, J.Q., Gai, X.D., Li, J. & Xiao, W.B. (2004) Two types of acid-sensing ion channel currents in rat hippocampal neurons. *Neurosci. Res.*, **50**, 493–499.
- Weng, J.Y., Lin, Y.C. & Lien, C.C. (2010) Cell Type-Specific Expression of Acid-Sensing Ion Channels in Hippocampal Interneurons. *J. Neurosci.*, **30**, 6548–6558.
- Williams, R.H., Jensen, L.T., Verkhratsky, A., Fugger, L. & Burdakov, D. (2007) Control of hypothalamic orexin neurons by acid and CO₂. *Proc. Natl Acad. Sci. USA*, **104**, 10685–10690.
- Xiong, Z.G., Zhu, X.M., Chu, X.P., Minami, M., Hey, J., Wei, W.L., MacDonald, J.F., Wemmie, J.A., Price, M.P., Welsh, M.J. & Simon, R.P. (2004) Neuroprotection in ischemia: blocking calcium-permeable acid-sensing ion channels. *Cell*, **118**, 687–698.
- Zhou, M., Xu, G., Xie, M., Zhang, X., Schools, G.P., Ma, L., Kimelberg, H.K. & Chen, H. (2009) TWIK-1 and TREK-1 are potassium channels contributing significantly to astrocyte passive conductance in rat hippocampal slices. *J. Neurosci.*, **29**, 8551–8564.
- Ziemann, A.E., Schnizler, M.K., Albert, G.W., Severson, M.A., Howard, M.A. III, Welsh, M.J. & Wemmie, J.A. (2008) Seizure termination by acidosis depends on ASIC1a. *Nat. Neurosci.*, **11**, 816–822.